Supporting Material for

Compressive spatial summation in human visual cortex

Kendrick N. Kay, Jonathan Winawer, Aviv Mezer, Brian A. Wandell

Journal of Neurophysiology, doi:10.1152/jn.00105.2013

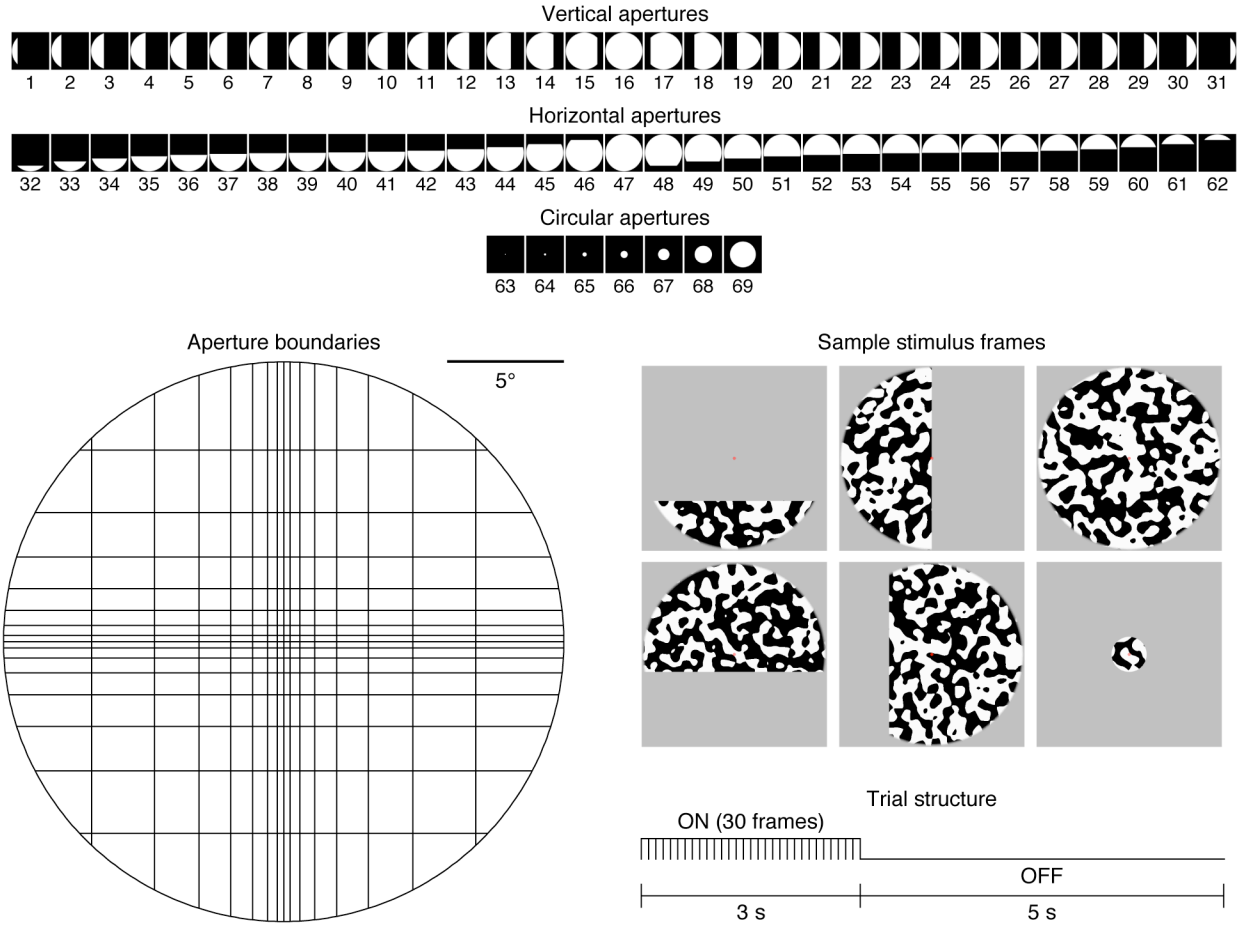

Supporting Fig. A. Schematic of stimuli used in the main experiment (datasets 1–3). Stimuli consisted of contrast patterns seen through vertical, horizontal, and circular apertures. Apertures were bounded by vertical and horizontal cuts through the visual field. During the first three seconds of a trial, the subject viewed contrast patterns through one of the apertures; for the remaining five seconds, the subject viewed the neutral-gray background.

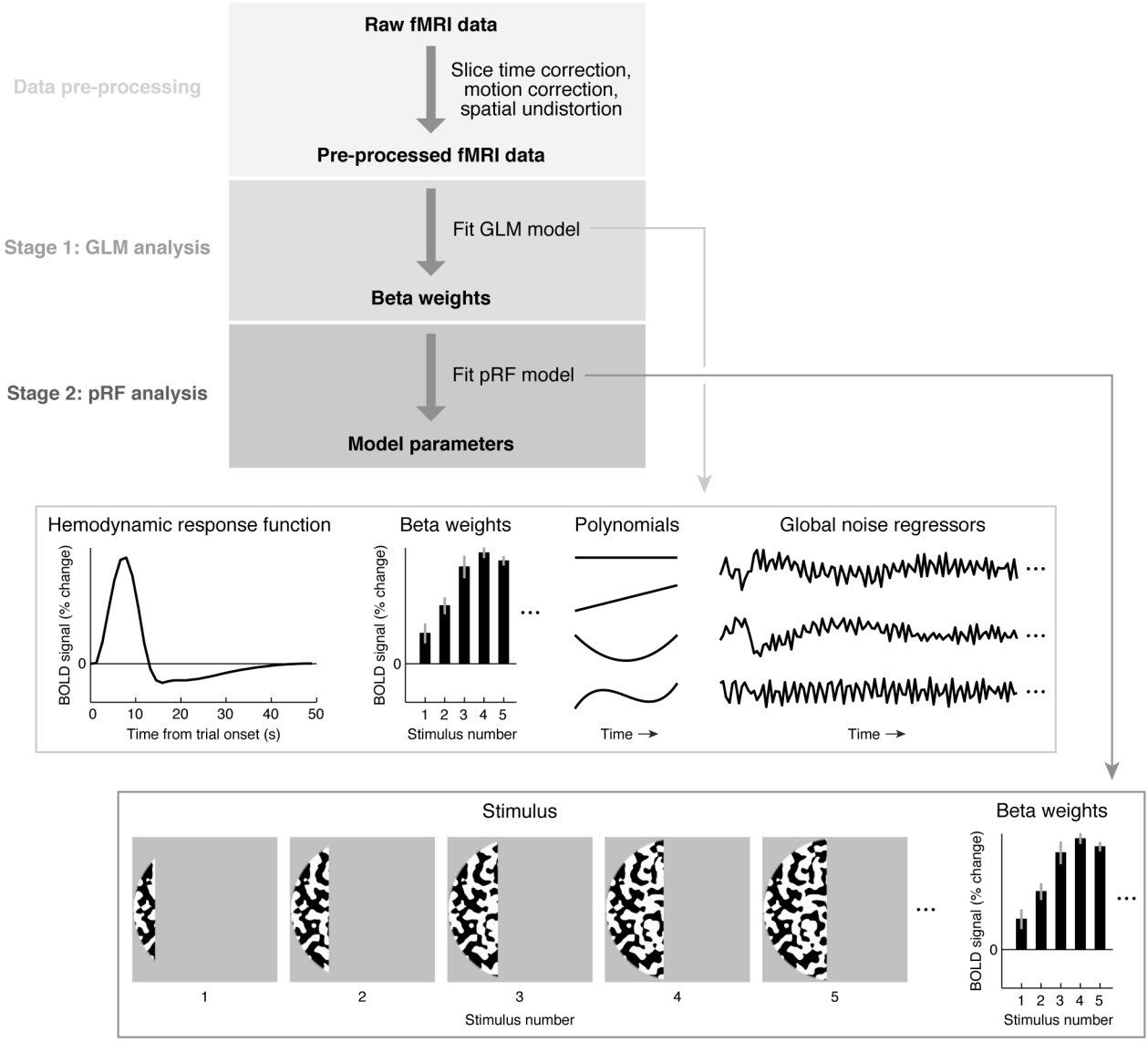

Supporting Fig. B. Summary of analysis workflow. The raw fMRI data are pre-processed to correct differences in slice acquisition times, head motion, and spatial distortion. The data are then analyzed in two stages. In the first stage, the time-series data are analyzed using a general linear model (GLM). The GLM consists of a hemodynamic response function, beta weights (representing the amplitude of the BOLD response to each stimulus), polynomial regressors, and global noise regressors. In the second stage, a population receptive field (pRF) model is fit to the beta weights obtained for each voxel. The pRF model characterizes the relationship between the stimuli shown to the subject and the obtained beta weights (see Fig. 5 for details). Fitting the pRF model yields a set of model parameters that characterize the response properties of each voxel.

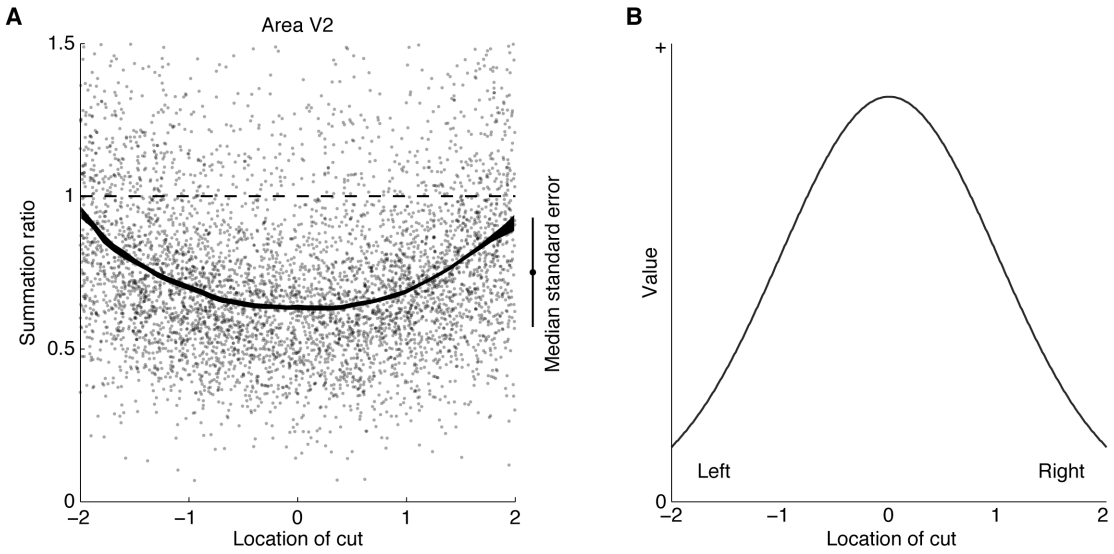

Supporting Fig. C. Details of spatial summation tests. Here we illustrate summation tests for an example case (V2, vertical apertures). *A*: summation ratios as a function of location. Each gray dot represents one spatial summation test for one voxel using a pair of vertical apertures. The *x*-axis indicates the horizontal position of the visual field cut that bounds the apertures, and is relative to the pRF center in units of pRF size (see panel B). The error bar to the right of the plot indicates the median standard error across summation tests. The solid line is a smooth curve fitted to the data points using local linear regression (Hastie et al. 2001) and an L_1 error metric (the width of the line indicates standard error). The dotted line indicates a summation ratio of one, which corresponds to linear spatial summation. Summation ratios approach one for cuts that are far from the pRF center because for these cuts, one of the partial apertures is too distant to evoke a substantial response and so summation holds trivially. *B*: location of visual field cuts relative to pRFs. The black line is a horizontal profile through the 2D Gaussian that describes the response of a pRF to point stimuli (see Methods). The locations of visual field cuts are expressed in terms of number of standard deviations of the 2D Gaussian away from the center of the Gaussian.

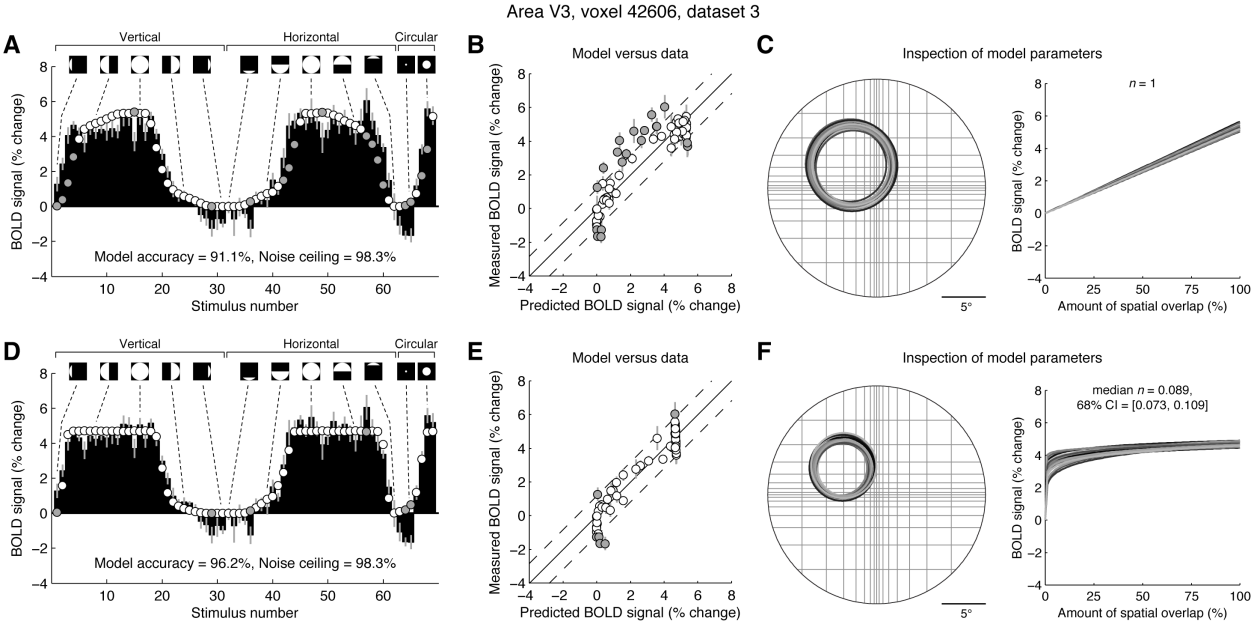

Supporting Fig. D. Data and model fits for an example voxel. *A–C*: inspection of linear model. In panel A, black bars indicate the measured BOLD responses to the apertures (depicted by small icons). Leave-one-out cross-validation was used to fit the model, and circles indicate the responses predicted by the model. Filled circles indicate predictions that differ significantly from the measured responses ($p < 0.01$; pooled estimate of standard error; two-tailed z-test). The linear model does fairly well but exhibits systematic undershoots and overshoots. In panel B, the predictions of the linear model are plotted against the data. The dotted line indicates the threshold beyond which predictions differ significantly from the data. A compressive nonlinear relationship between the model and the data is evident. In panel C, the parameters obtained in different bootstraps of the model are shown. On the left are circles representing pRF location, superimposed on top of a depiction of the stimulus extent and the aperture boundaries. On the right are curves representing the static nonlinearity, with the x-axis indicating the amount of spatial overlap between the stimulus and the pRF relative to that obtained with a full-field aperture. *D–F*: inspection of CSS model (format same as panels A–C). The CSS model describes the data more accurately than the linear model.

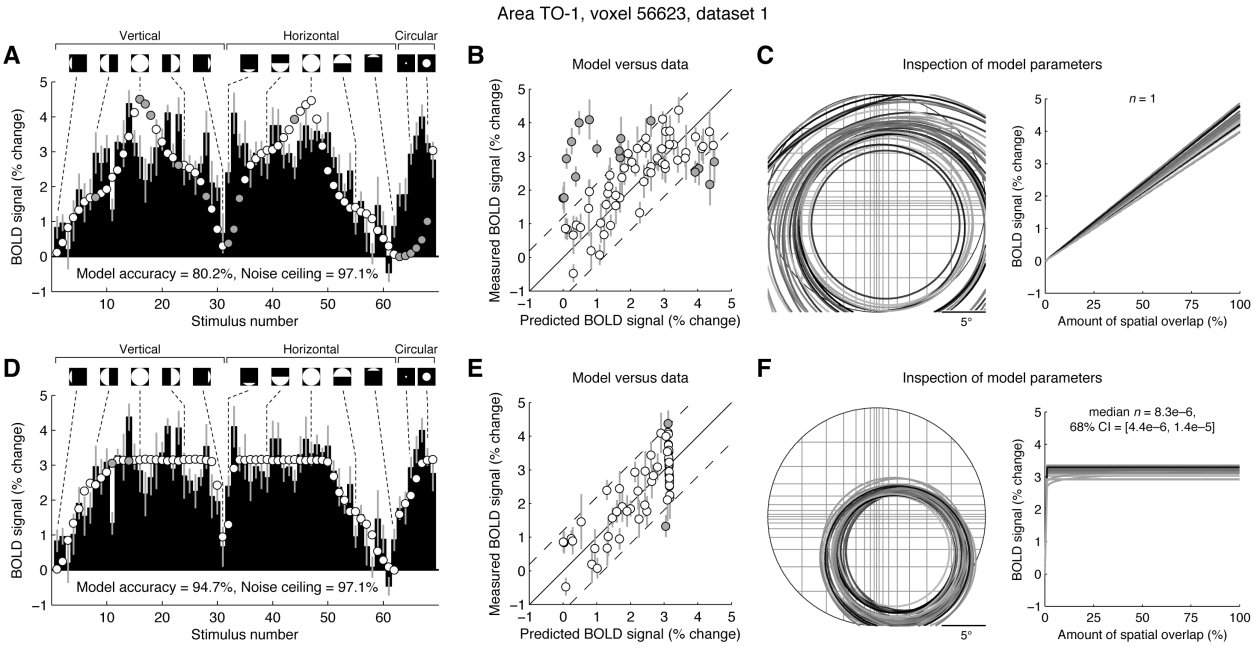

Supporting Fig. E. Data and model fits for another example voxel. Format same as in Supporting Fig. D. The CSS model predicts a uniform response across a wide range of apertures; this is due to the combination of large pRF size and small pRF exponent.

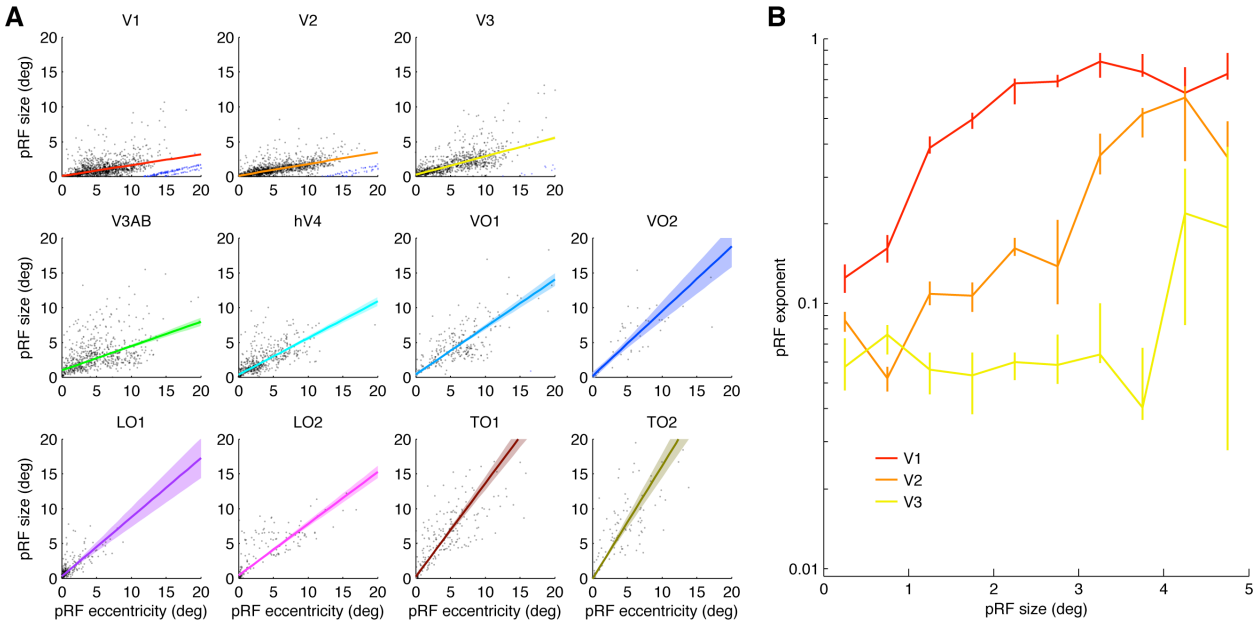

Supporting Fig. F. Details of model parameters. *A*: eccentricity versus size. This panel shows the individual data points used to generate the lines relating eccentricity and size in Fig. 7A. Data points are partially transparent, which causes regions with high data density to become dark. For each visual field map, we fit a line minimizing the sum of the perpendicular distances from the data points to the line. To reduce the influence of outliers and artifacts, we restricted the fitting procedure to a range covering most of the data points (0–20 deg for eccentricity, 0–20 deg for size) and excluded cases where less than 0.01 of the pRF overlaps the stimulus (these cases are indicated in blue). The fitting procedure was bootstrapped to estimate standard error, indicated by the band around each line. *B*: changes in exponent are distinct from changes in size. The existence of a range of pRF sizes within individual visual field maps allows us to compare exponents across maps while holding size constant. In this panel we bin voxels by size and plot the median exponent in each bin. Even after controlling for size, exponents decrease from V1 to V2 to V3.

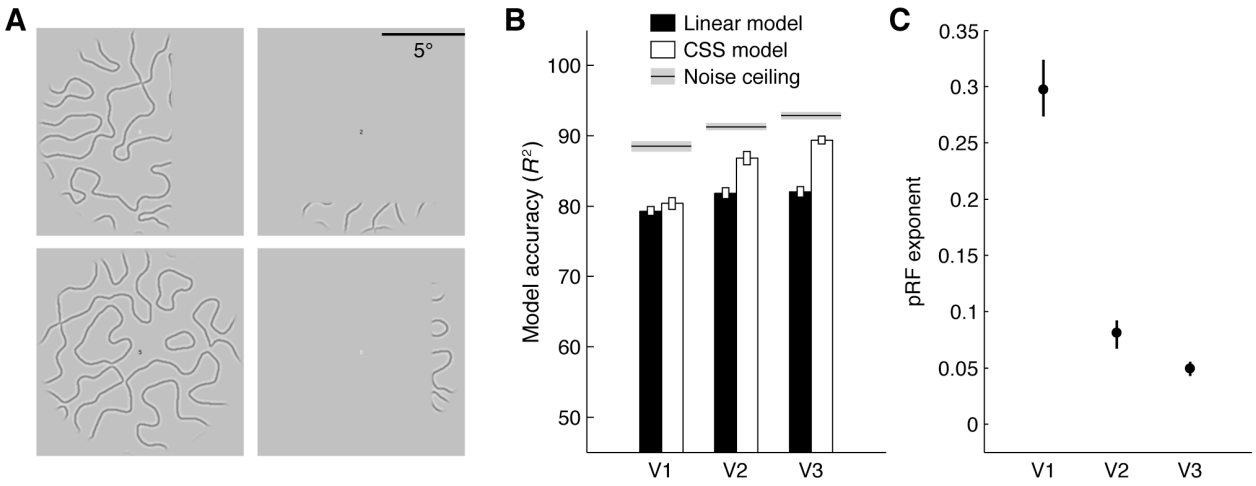

Supporting Fig. G. Replication of main experiment using alternative contrast patterns. As a further demonstration that compressive spatial summation (CSS) is not a trivial consequence of luminance edges between the contrast patterns and the gray background, we repeated the full set of measurements of the main experiment (69 spatial apertures) using band-pass contrast patterns. *A*: sample stimulus frames. *B*: cross-validation accuracy. Format same as in Fig. 6A. The CSS model again outperforms the linear model. *C*: changes in pRF exponent. The median exponent in each map is plotted, with error bars indicating 68% confidence intervals. The compressive nonlinearity is again more pronounced in extrastriate maps.

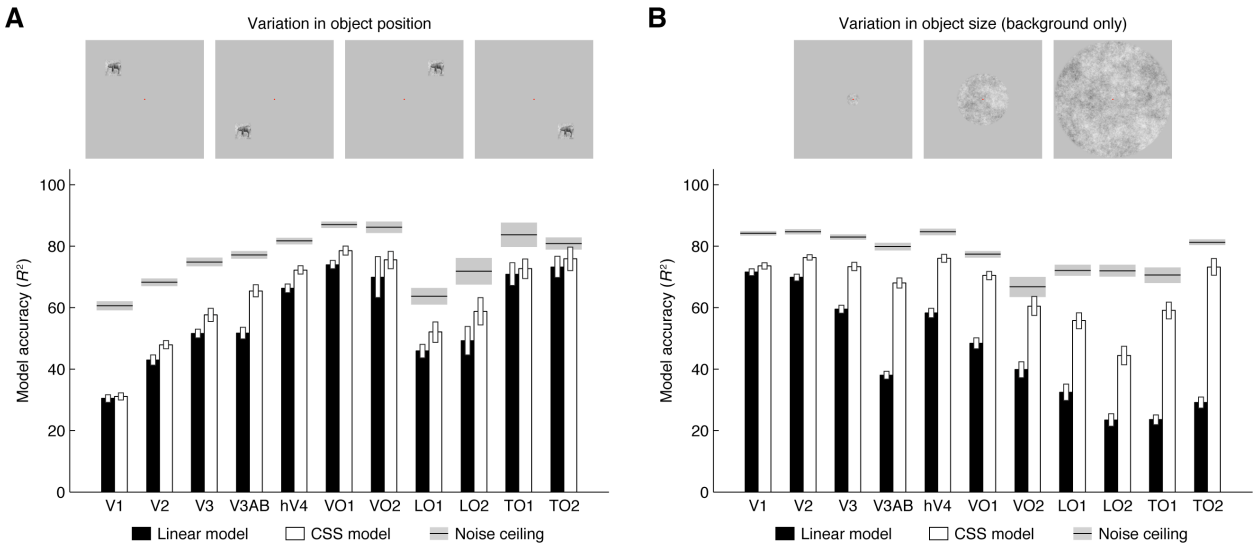

Supporting Fig. H. Additional object experiments. We performed two additional object manipulations besides the object-size manipulation shown in Fig. 8. *A*: variation in object position. Objects were presented within square apertures at a variety of positions. This manipulation tests spatial summation because the spatial overlap between a stimulus and a pRF changes with the position of the stimulus. However, the amount of variation in spatial overlap is smaller than that obtained when varying the size of the stimulus, which explains why the performance improvement provided by the CSS model for variation in position is less than the improvement for variation in size. The low noise ceilings in V1 and V2 can be attributed to the fact that individual voxels in these areas have small pRFs and respond to only a few of the stimuli. *B*: variation in object size (background only). This is the same as the original object-size manipulation, except that the objects themselves are omitted. Noise ceilings are lower than in the original manipulation, reflecting the fact that responses are weaker when only the background is presented.

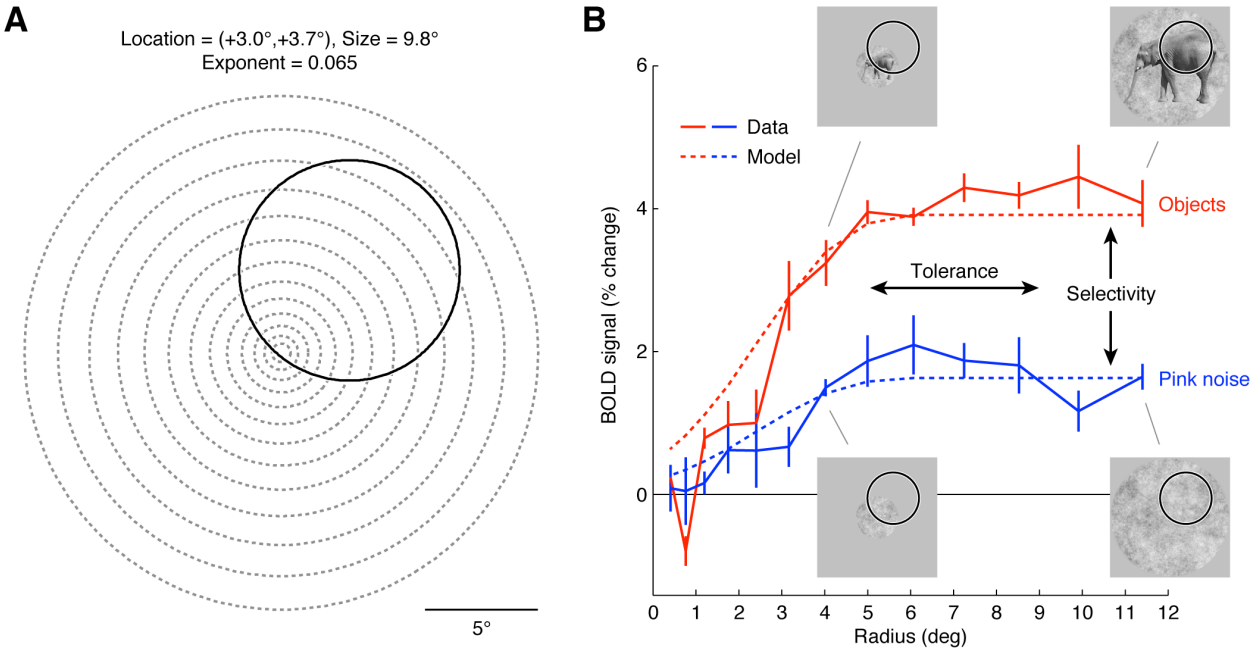

Supporting Fig. I. CSS model is compatible with the selectivity-tolerance framework. *A*: schematic of stimuli and model. We measured responses to stimuli placed within circular apertures of different sizes (dotted lines; same apertures as in Fig. 8). The pRF estimate for an example voxel in hV4 is shown (black circle). Note that this voxel has been selected to demonstrate a proof of concept and is not intended to represent the main findings of this study. *B*: size responses and model predictions. Two types of stimuli were used, objects and pink noise. The response of the example voxel to each stimulus type is plotted as a function of aperture radius. Notice that the voxel response to each stimulus type is relatively constant over a wide range of sizes (tolerance) and that preference for objects is maintained over this range (selectivity). The prediction of the pRF (as illustrated in panel A) is also plotted. Since the CSS model does not address stimulus selectivity, it cannot predict the gain of the responses. We have, for visualization purposes, scaled the pRF prediction separately for each stimulus type to fit the data. A direction for future research is to extend the CSS model to explicitly account for stimulus selectivity.

Dataset	*Subject*	*Stimulus*	*Modifications to experimental design*	*Stimulus size / Viewing distance*	*Scanner*	*RF coil*	*Number of global noise regressors*
1	1	Contrast patterns	none	29.5° / 20 cm	3T1	Nova 8-channel surface coil	2
2	2	Contrast patterns	none	23.5° / 23 cm	3T1	Nova quadrature surface coil	5
3	3	Contrast patterns	none	24.7° / 23 cm	3T1	Nova quadrature surface coil	5
4	2	Modified contrast patterns and object-position manipulation	null trial inserted after every six stimulus trials	25.1° / 23.5 cm	3T1	Nova quadrature surface coil	5
5	3	Modified contrast patterns and object-position manipulation	null trial inserted after every six stimulus trials	25.4° / 22 cm	3T1	Nova quadrature surface coil	5
6	4	Modified contrast patterns and object-size manipulation	null trial inserted after every six stimulus trials	21.2° / 24 cm	3T1	Nova quadrature surface coil	5
7	5	Modified contrast patterns and object-size manipulation	null trial inserted after every six stimulus trials	22.8° / 26 cm	3T1	Nova quadrature surface coil	3
"	"	Modified contrast patterns presented at low contrast	two runs consisting of only horizontal apertures	"	"	"	3
"	"	Modified contrast patterns in a slow event-related design	two runs consisting of three vertical apertures (Full, Left, Right) presented in fixed order; 3-s ON, 25-s OFF trial structure	"	"	"	3
8	3	Alternative contrast patterns	seven runs consisting of three horizontal apertures (Bottom, Top, Full) and several types of contrast patterns	12.6° / 182 cm	CNI	Nova 32-channel head coil	4
9	2	Alternative contrast patterns	3-Hz image rate (duty cycle: 167-ms ON / 167-ms OFF); each stimulus presented six times	12.5° / 183 cm	CNI	Nova 32-channel head coil	3
10	4	Alternative contrast patterns	3-Hz image rate (duty cycle: 167-ms ON / 167-ms OFF); each stimulus presented three times	12.7° / 180 cm	CNI	Nova 32-channel head coil	5

Supporting Table A. Summary of all datasets.
3T1 = Lucas Center at Stanford University, GE Signa HDx 3.0T scanner
CNI = Stanford Center for Neurobiological Imaging, GE Signa MR750 3.0T scanner

	Median ratio between response to full aperture at high contrast and response to full aperture at low contrast	*Median ratio between response to full aperture containing objects and response to full aperture containing contrast patterns*
V1	212%*	71%
V2	130%*	92%
V3	127%*	117%*
V3AB	103%*	150%*
hV4	144%*	144%*
VO-1	116%*	184%*
VO-2	104%*	224%*
LO-1	111%*	176%*
LO-2	121%*	216%*
TO-1	102%*	209%*
TO-2	111%*	162%*

Supporting Table B. Summary of response-ceiling control experiments. This table summarizes the results of the low-contrast experiment described in Fig. 3B and the object experiment described in Fig. 3C. Ratios marked with an asterisk (*) are significantly larger than 100% ($p < 0.05$, two-tailed sign test). The two experiments demonstrate complementary effects: posterior visual field maps generally exhibit a large increase in response at high contrast (compared to low contrast), whereas anterior visual field maps generally exhibit a large increase in response for objects (compared to contrast patterns). Together, these results provide evidence that sub-additivity is not due to a response ceiling.